ISIJ International, Vol. 52 (2012), No. 5, pp. 874–883

Microstructure Control during Fabrication of Ultrafine Grained Dual-phase Steel: Characterization and Effect of Intercritical Annealing Parameters

Marion CALCAGNOTTO,[1)] Dirk PONGE[2)]* and Dierk RAABE[2)]

1) Formerly at Max-Planck-Institut für Eisenforschung GmbH. Now at Salzgitter Mannesmann Forschung GmbH, Materials and Process Development, Eisenhüttenstraße 99, Salzgitter, 38239 Germany. E-mail: m.calcagnotto@sz.szmf.de
2) Max-Planck-Institut für Eisenforschung GmbH, Max-Planck-Straße 1, Düsseldorf, 40237 Germany. E-mail: d.ponge@mpie.de, d.raabe@mpie.de

(*Received on September 13, 2011; accepted on December 15, 2011*)

An ultrafine grained (UFG) ferrite/cementite steel was subjected to intercritical annealing in order to obtain an UFG ferrite/martensite dual-phase (DP) steel. The intercritical annealing parameters, namely, holding temperature and time, heating rate, and cooling rate were varied independently by applying dilatometer experiments. Microstructure characterization was performed using scanning electron microscopy (SEM) and high-resolution electron backscatter diffraction (EBSD). An EBSD data post-processing routine is proposed that allows precise distinction between the ferrite and the martensite phase. The sensitivity of the microstructure to the different annealing conditions is identified. As in conventional DP steels, the martensite fraction and the ferrite grain size increase with intercritical annealing time and temperature. Furthermore, the variations of the microstructure are explained in terms of the changes in phase transformation kinetics due to grain refinement and the manganese enrichment in cementite during warm deformation.

KEY WORDS: grain refinement; dual-phase steel; ultrafine grains; EBSD; microstructure evolution.

1. Introduction

Grain refinement in steels is an effective way for property optimization, as it is the only strengthening mechanism that increases yield and tensile strength, and lowers the ductile-to-brittle transition temperature simultaneously. In recent years, a variety of processing routes has been developed which aim at the production of ultrafine grained (UFG) steels with a ferrite grain size of 1 μm and below, which are well summarized in the review of Song *et al*..[1)] However, most of these UFG ferrite/cementite steels are characterized by a very low strain hardening rate and consequently, a low uniform elongation, when compared to their coarse grained counterparts.[2,3)] Among the different attempts to restore the strain hardening capacity of UFG steels,[4–6)] the replacement of cementite by martensite through an intercritical annealing treatment seems to be most efficient.[7,8)] During intercritical annealing in the ferrite + austenite two-phase field, the desired amount of austenite is formed. Upon rapid cooling, the austenite transforms into martensite. These so produced UFG ferrite/martensite dual-phase (DP) steels are of special interest for industrial applications, as conventional coarse and fine grained DP steels have been studied for more than three decades[9–19)] and make up a considerable portion of today's car bodies.[20)] It has been repeatedly demonstrated that increasing the strength of DP steels by grain refinement is not counteracted by a significant loss of tensile ductility.[7,8,16,17,21)] This is attributed to the increase in the strain hardening rate,[7,8,17)] the change in dislocation distribution[7,22)] and to the enhancement of martensite plasticity.[21)]

UFG DP steels have been produced by applying different processing routes, yet, the number of studies on this new material is still limited. Son *et al*.[7)] produced UFG DP steels with and without vanadium additions by equal channel angular pressing (ECAP) plus intercritical annealing and studied the dislocation distribution in UFG ferrite and its effect on the tensile properties. Delincé *et al*.[23,24)] used cold swaging plus intercritical annealing to produce DP steels of varying grain sizes and analyzed the different strengthening contributions and the resulting mechanical properties by nanoindentation and a grain-size dependent strain hardening model. Mukherjee *et al*.[25)] proposed a processing route based on deformation-induced ferrite transformation (DIFT) and studied the effect of molybdenum and niobium on microstructure evolution. In two previous studies, we demonstrated that UFG DP steels can be produced by large strain warm deformation followed by intercritical annealing[26)] and clarified the critical importance of a certain manganese content on microstructure evolution.[26,27)] However, there is a lack of systematic studies on the processing parameters that control the microstructure evolution in UFG DP steels. In contrast, the microstructure evolution during intercritical annealing was extensively studied in coarse grained DP steels that were produced by conventional hot

and/or cold rolling.[10,28–36] However, phase transformation kinetics are altered due to grain refinement as a result of the higher density of potential nucleation sites and the change in cementite morphology from a pearlitic lamellar structure to a spheroidal shape. Furthermore, microstructure evolution depends on the dislocation content and distribution and thus, on the thermomechanical history of the material.

As the mechanical properties are directly related to the microstructure parameters such as grain size, phase fractions, fraction of high-angle grain boundaries (HAGBs), precipitations, interstitial content *etc*., the careful control of the microstructure is a prerequisite for the development of a new material. With respect to the limitations in the variation of processing conditions in industrial annealing facilities, it is of critical importance to identify the sensitivity of the microstructure evolution to the variation of the processing variables. Therefore, the crucial intercritical annealing parameters (heating rate, holding temperature, holding time, and cooling rate) applied in the processing route to obtain UFG DP steels are systematically varied in the present study. The aim is to define the microstructure controlling mechanisms during intercritical annealing in order to tailor an optimized microstructure.

For the precise determination of the phase fractions, the ferrite grain size, and the fraction of HAGBs in ferrite, we apply high-resolution electron backscatter diffraction (EBSD) and propose an EBSD data post-processing routine that accounts for the high fraction of grain boundaries that generally complicate microstructure characterization.

2. Experimental Procedures

2.1. Materials Processing

The chemical composition of the steels used was (in wt.%) 0.17 C, 1.63 Mn, 0.28 Si, 0.036 Al, 0.0021 P, 0.0038 S, 0.0025 N, the balance being Fe. A lean composition was chosen in order to show that an ultrafine grained ferrite/martensite microstructure can be obtained without microalloying elements that promote grain refinement (*e.g*. V, Nb) and without alloying elements that increase the hardenability (*e.g*. Cr, Mo). However, a certain Mn content was shown to be beneficial for obtaining the desired microstructure.[26,27] The steel was produced by vacuum induction melting. The cast ingot was cut into rectangular laboratory samples of $50 \times 40 \times 60$ mm^3. For materials processing, a large scale 2.5 MN hot deformation simulator located at the Max-Planck-Institut für Eisenforschung was used.[37,38] This computer controlled servohydraulic press allows simulating industrial thermomechanical processing routes by performing multistep flat compression tests. The processing schedule is outlined in **Fig. 1**. The first processing step simulates conventional hot deformation. The samples were austenitized for 3 min at 934°C, deformed with a strain of 0.3 and then cooled to the pearlite finish temperature at a rate of –8 K/s. In order to refine the microstructure down to the μm scale, large strain warm deformation was applied, exerting a four-step flat compression series at 550°C with a total strain of 1.6. Subsequently, the samples were annealed at 550°C for 2 h to simulate elevated coiling temperatures. The resulting microstructure is an ultrafine grained ferrite (F) matrix with homogeneously distributed spheroidized cementite (C) particles (UFG-F/C steel). Details of the thermomechanical processing and the microstructure evolution during large strain warm deformation are described in.[39]

The final ferrite/martensite dual phase structure was produced by an intercritical annealing treatment in the ferrite + austenite two-phase region followed by quenching. This treatment was performed in a Bähr Dil 805 A/D quenching and deformation dilatometer using cylindrical samples with a length of 10 mm and a radius of 4 mm. The center of the samples corresponds to the position in the warm deformed specimen where the local strain equals the nominal strain as was elaborated by evaluating the distribution of local strain in the deformed zone.[40] The dilatometer allows the careful control of the temperature during heating, holding and cooling which is essential to obtain reliable results about the effect of the intercritical annealing conditions. The sample is heated in an induction coil. During the annealing treatment, the temperature and the change in length of the specimen are continuously recorded. The temperature is controlled via a thermocouple that is spot welded on the sample surface. The precise determination of the change in length is guaranteed by a glass gauge that connects the sample with the measuring unit. For cooling, hydrogen gas was used, reaching a maximum cooling rate of –140 K/s between the annealing temperature and room temperature. As this technique does not allow large specimen suitable for tensile testing to be used, the mechanical properties of the specimen cannot be determined. However, implications for the mechanical properties can be derived to some extent from the martensite fraction, size and distribution, as well as from the ferrite grain size.

2.2. Microstructure Characterization

Samples for electron backscatter diffraction (EBSD) investigations were prepared by standard mechanical grinding and polishing procedures, finishing with 3 min polishing with colloidal silica. EBSD experiments were conducted using a JEOL JSM 6500F high-resolution, high intensity scanning electron microscope (SEM) equipped with field emission gun (FEG). A high speed DigiView CCD camera was used for pattern acquisition. Data was recorded and analyzed using the EDAX-TSL OIM Analysis* software package. Martensite was indexed as body-centered cubic (bcc) phase and is distinguished from ferrite by its lower Image Quality (IQ) and Confidence Index (CI) which is due to the higher crystal lattice imperfection.

EBSD data provide information about the grain size, grain shape, and grain boundary character which allow important correlations with the mechanical properties to be drawn. The TSL software package provides the grain size distribution of different phases that have been recorded. However, in the current case martensite has the same crystal structure as ferrite with the only difference being the tetragonal distortion of the martensite lattice. Thus, the separation of martensite and ferrite is not accomplished automatically. For a reliable microstructure characterization, a careful distinction between martensite and ferrite is required. As mar-

*OIM Analysis is a trade mark of EDAX/TSL, Draper, UT.

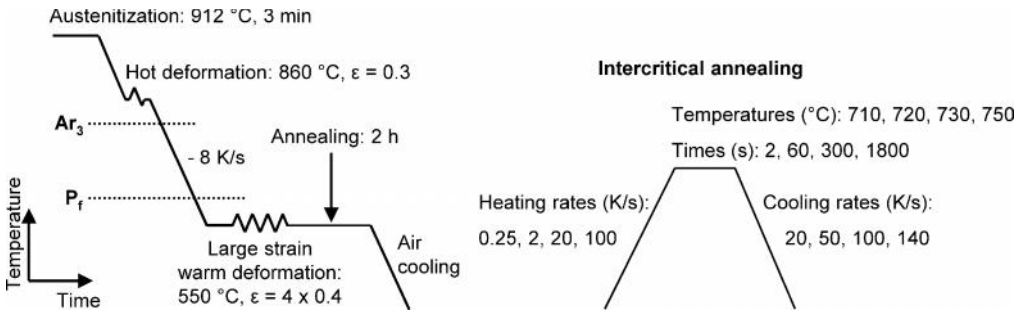

Fig. 1. Processing route to obtain ultrafine grained ferrite/martensite dual-phase steel. The intercritical annealing conditions studied are indicated. Ar_3: Non-equilibrium ferrite formation start temperature during cooling, P_f: pearlite formation finish temperature, ε: logarithmic strain.

tensite contains a higher number of dislocations than ferrite, indexing of martensite is based on weaker peaks in Hough space and is associated with higher uncertainty. This is reflected in the frequency distribution of the Image Quality and the Confidence Index which in general show a double-peak shape.

Figure 2 shows an exemplary IQ histogram of a UFG DP steel investigated in this study. The lower martensite peak at low IQ values can be clearly distinguished from the higher ferrite peak at high IQ values. By simply defining a threshold value, the phases can roughly be separated. This method was applied by Wilson *et al*.[41] using the IQ value and by Waterschoot *et al*.[42] using the CI. However, the definition of a threshold value is subjective and it varies depending on factors such as sample preparation and scanning accuracy. Furthermore, the grain boundaries also exhibit low IQ and CI values and hence, are added to the martensite fraction. Therefore, the martensite fraction is overestimated. Wu *et al*.[43] developed a multi-peak model that is capable of splitting the IQ frequency distribution into peaks stemming from phases with different dislocation content and from grain boundaries. However, in this method, the authors clear the dataset for grain boundary regions, *i.e*. all measurement points adjacent to the grain boundaries are excluded from the analysis. Depending on the ratio between grain size and step size, a large fraction of the grains is discarded in this way. If the phase fractions are not equal, as it is normally the case, a higher fraction of the major phase is subtracted than of the minor phase. As a consequence, the minor phase fraction (usually martensite) is again overestimated. For these reasons, a new method was developed that overcomes these difficulties.

Figure 3(a) shows the IQ map that corresponds to the IQ histogram in Fig. 2. Martensite appears dark due to the low pattern quality, ferrite appears bright. The grain boundaries show intermediate or low values. In the first step, the IQ threshold value is automatically defined as the minimum between the martensite peak and the ferrite peak, indicated by the dashed line in Fig. 2. This value proved to be suitable as a first approximation, because within the trough between the peaks, the integrated volume fraction of ferrite varies only slightly (solid line in Fig. 2). Then, all measurement points with an IQ below this threshold are defined as martensite. After this step, the martensite fraction includes some of the grain boundaries, Fig. 3(b). In order to remove these pixels from the martensite fraction, a second step was implemented in the routine. A pixel (viz. a measurement point) is only assigned to the martensite fraction if at least three neighboring points of this pixel also have an IQ value below the threshold value. In this way, the scattered boundary points are excluded from the martensite fraction, Fig. 3(c). Comparing Figs. 3(a) with 3(c) reveals very good agreement between the shapes of the martensite islands. Small amounts of retained austenite occur frequently in the material, especially between the martensite laths. As its IQ value is generally lower than the threshold value, the determined martensite fraction is strictly speaking the second phase fraction consisting of martensite and retained austenite. Therefore, the retained austenite fraction was additionally determined from the unprocessed data. The true martensite fraction is then the difference between total martensite/austenite (M/A) fraction and the retained austenite fraction. However, as the amount of retained austenite is generally small and mainly occurs within the martensite islands, the M/A constituent phase will be hereafter simply referred to as 'martensite' in the text.

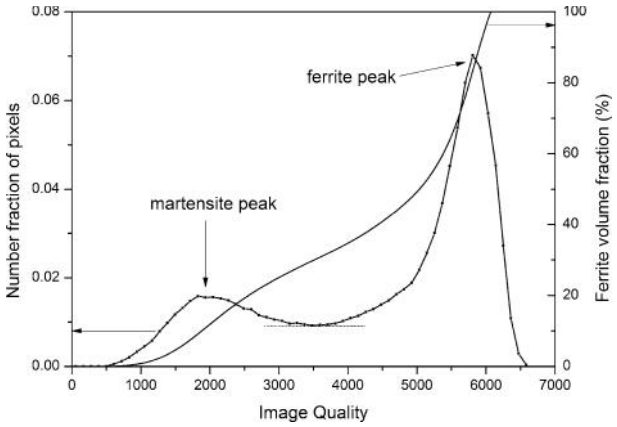

Fig. 2. Exemplary Image Quality distribution of a UFG DP steel and corresponding integrated ferrite volume fraction.

Once the phase separation is accomplished, the grain size determination can be realized with the standard procedures offered in the TSL software package. In the present case, the mean linear intercept (MLI) length was selected to define the grain size, with the minimum misorientation angle that defines a grain boundary being 2°. The MLI length was determined both in the compression direction and in the rolling direction and is given as the average of both values. From the separated phase fractions, the fraction of high-

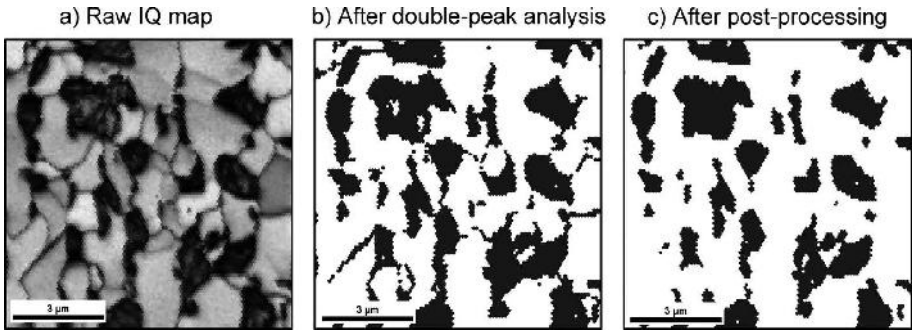

Fig. 3. Phase separation based on EBSD measurements. (a) Exemplary section of an Image Quality (IQ) map, (b) martensite fraction (dark grey) based on the double-peak analysis of the raw IQ chart (Fig. 2), (c) martensite fraction after post-processing that discards the grain boundaries.

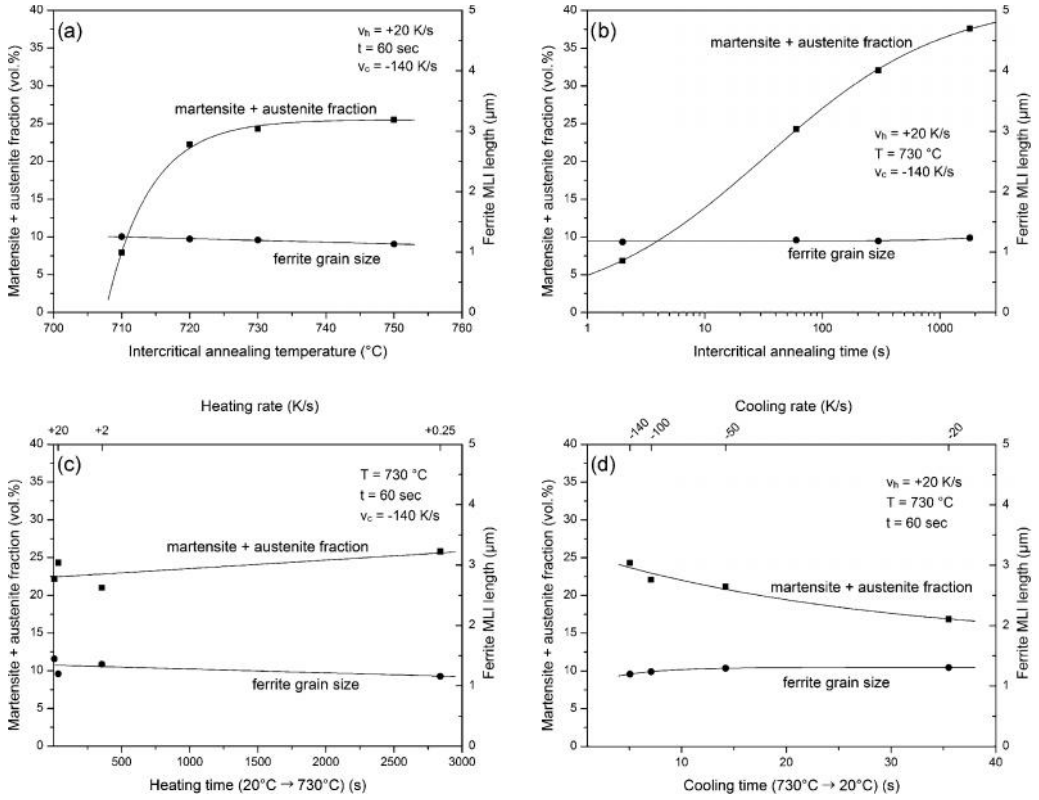

Fig. 4. Influence of the intercritical annealing parameters (a) holding temperature, (b) holding time, (c) heating rate and (d) cooling rate on martensite + austenite volume fraction and ferrite grain size (mean linear intercept length, MLI). v_h: heating rate, T: annealing temperature, t: holding time, v_c: cooling rate.

angle grain boundaries (HAGBs) was additionally identified. The HAGB fraction is of considerable importance for the toughness of a material, as HAGBs are more resistant to cleavage crack propagation than low-angle grain boundaries (LAGBs).[44] Here, only the HAGB fraction of the ferrite-ferrite grain boundaries was determined, the ferrite-martensite phase boundaries were excluded from the calculation. The ferrite aspect ratio is defined as the MLI length in the rolling direction divided by the MLI length in the compression direction. As the martensite is partly interconnected, a definite martensite island size is not defined. Two EBSD scans were performed on each specimen at a step size of 100 nm, covering $50 \times 100\,\mu m^2$ in total, and the average values are given. In this way, at least 2 000 grains per sample were analyzed.

3. Results and Discussion

3.1. Effect of Holding Temperature

During heating, the ferrite + cementite → austenite phase transformation starts at the Ac_1 temperature (non-equilibrium austenite formation start temperature) and finishes at the Ac_3 temperature (non-equilibrium austenite formation finish temperature). These temperatures mark the borders of the non-equilibrium ferrite + austenite two-phase field, *i.e.* of the intercritical annealing temperature range. They were determined using dilatometer tests.[26] In the dilatometer test, the change in length and the temperature are recorded continuously during heating. Deviations from linearity reflect the onset or the completion of phase transformation. In the present material, austenite formation starts at around 721°C (Ac_1) and finishes at 835°C (Ac_3). Austenite formation takes

place in two steps. 1) Rapid dissolution of cementite in the ferrite + cementite + austenite three-phase field and 2) slower growth of austenite at the expense of ferrite in the ferrite + austenite two-phase field.

To study the influence of the holding temperature, samples were heated at a rate of +20 K/s to 710°C, 720°C, 730°C and 750°C, held for 1 min and then quenched at a rate of –140 K/s to room temperature. Due to the fast quenching rate, the formation of epitaxial ferrite is widely suppressed. Therefore, it is assumed that the observed martensite fraction is nearly equivalent to the austenite fraction at the intercritical annealing temperature just before quenching. **Figure 4**(a) shows the effect of the intercritical annealing temperature on the martensite volume fraction and the ferrite grain size. After the lowest tested temperature (710°C), the martensite fraction (strictly speaking the martensite + retained austenite (M/A) fraction) is around 7.9 vol.%. With increasing temperature, it increases first rapidly and then more gradually to reach 25.5 vol.% at 750°C. This value is far below the equilibrium austenite volume fraction of 45.9 vol.% (calculated using Thermo-Calc,[45] version TCCR, database TCFE5), indicating that the holding time of 1 min is by far not enough to establish phase equilibrium. The ferrite grain size and aspect ratio (**Table 1**) are nearly invariant to the temperature increase. Both values decrease slightly with increasing martensite volume fraction. Retained austenite (RA) makes up only a small portion of the total second phase fraction. The fraction of HAGBs in ferrite is highest for the lowest martensite fraction.

Typical micrographs of the lowest and highest test temperature are depicted in **Figs. 5**(a) and 5(b). The higher martensite fraction in the right image is clearly visible. The sample annealed at 710°C contains small amounts of cementite particles, partly situated along the ferrite grain boundaries, partly in the ferrite grain interior (arrow). Even though this temperature does not fall within the three-phase field of the equilibrium phase diagram,[27] the presence of cementite indicates that 1 min holding time given at 710°C does not allow full dissolution of cementite.

Plotting the martensite fraction as a function of holding temperature (Fig. 4(a)) reveals that there is a nearly linear increase at higher temperatures as it is given by the lever rule in the two-phase region. At lower temperatures, however, the austenite formation is delayed, the martensite fraction being only 7.9 vol.% compared to 29.6 vol.% in equilibrium. This finding is consistent with the results of Garcia and DeArdo[28] and Speich *et al*.,[31] although the investigated microstructures are different. A possible explanation bases on the results of Hillert *et al*.,[46] who found that phase transformation at low temperatures is controlled by diffusion of substitutional elements, thus essentially by Mn diffusion. At higher temperatures, it is controlled by carbon diffusion. It is known that the diffusion coefficient of Mn in austenite is seven orders of magnitude lower than the diffusion coefficient of C in austenite.[31] Moreover, Mn lowers the activity of carbon, *i.e*. it delays carbon flux through austenite. This is of particular importance in the present case because it was observed that cementite is enriched in Mn during the course

Table 1. Variation of the microstructural parameters with intercritical annealing (IA) parameters. M/A: martensite plus retained austenite volume fraction, called 'martensite' in the text for simplicity, RA: retained austenite volume fraction, F-F HAGB: high-angle grain boundary fraction in the ferrite phase.

	Heating rate (K/s)	IA temperature (°C)	IA time (sec)	Cooling rate (K/s)	M/A (vol.%)	RA (vol.%)	Ferrite grain size (μm)	Ferrite aspect ratio	F-F HAGB (%)	Fig.
Initial microstructure	—	—	—	—	0	0	0.84	1.28	60.8	
Effect of IA temperature	+20	710	60	–140	7.9	0.4	1.25	1.74	54.3	5(a)
	+20	720	60	–140	22.3	0.7	1.21	1.55	45.9	
	+20	730	60	–140	24.3	1.2	1.20	1.46	49.1	
	+20	750	60	–140	25.5	1.4	1.13	1.38	44.3	5(b)
Effect of IA time	+20	730	2	–140	6.9	0.7	1.17	1.65	57.3	5(c)
	+20	730	60	–140	24.3	1.2	1.20	1.46	49.1	
	+20	730	300	–140	32.1	0.4	1.18	1.51	48.8	
	+20	730	1 800	–140	37.6	0.2	1.23	1.41	48.4	5(d)
Effect of heating rate	+0.25	730	60	–140	25.8	0.4	1.16	1.45	42.0	5(e)
	+2	730	60	–140	21.0	1.0	1.36	1.49	44.3	
	+20	730	60	–140	24.3	1.2	1.20	1.46	49.1	
	+100	730	60	–140	22.2	0.9	1.45	1.46	37.1	5(f)
Effect of cooling rate	+20	730	60	–140	24.3	1.2	1.20	1.46	49.1	5(g)
	+20	730	60	–100	21.8	0.3	1.24	1.69	57.3	
	+20	730	60	–50	20.9	0.2	1.29	1.53	53.8	
	+20	730	60	–20	16.9	1.7	1.31	1.58	47.7	5(h)

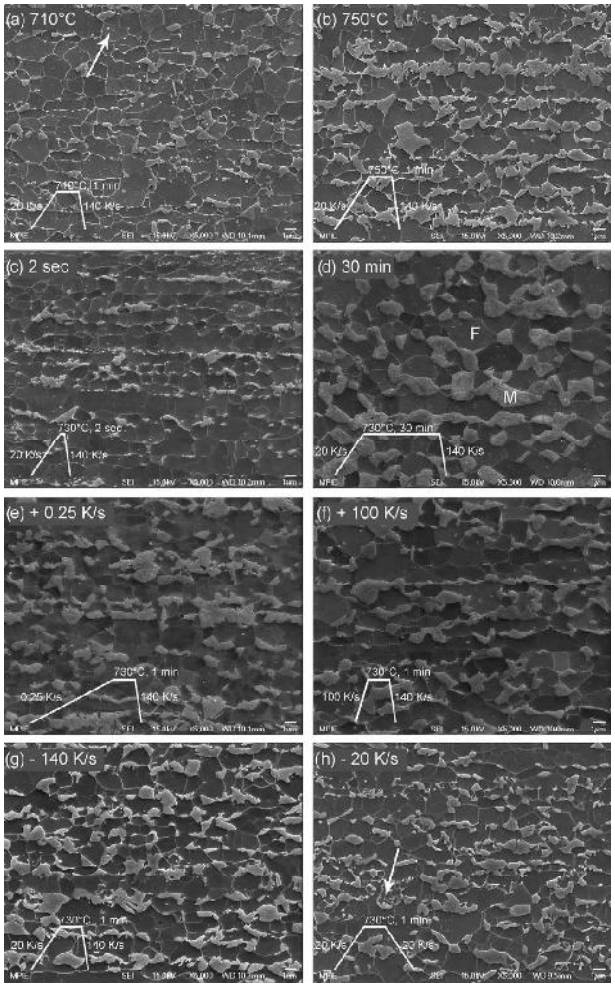

Fig. 5. Influence of the intercritical annealing conditions on microstructure evolution. Typical micrographs of the samples treated at the lowest and the highest intercritical annealing temperature (a, b), holding time (c, d), heating rate (e, f) and cooling rate (g, h) reveal the different effects of these parameters on ferrite (F) grain size and martensite (M) volume fraction. Magnification is the same in all images. Rolling direction is horizontal, normal direction is vertical. See Table 1 and text for details.

of large strain warm deformation.[47] For these reasons, phase transformation and austenite growth are sluggish at low temperatures and the resulting martensite fraction is small. At higher temperatures, phase transformation is controlled by carbon diffusion, Mn diffusion playing a minor role. This is partially explained by the higher carbon supersaturation in austenite at higher temperatures.[48] The carbon-diffusion controlled process leads to much faster growth kinetics and consequently to a higher martensite fraction.

3.2. Effect of Holding Time

Samples were heated at a rate of +20 K/s to 730°C and held for different times between 2 sec and 30 min before they were quenched to room temperature at a rate of –140 K/s. The effect of intercritical holding time on microstructure characteristics is shown in Fig. 4(b) and Table 1.

The ferrite + cementite → austenite transformation proceeds very fast during the first seconds. A holding time of 2 seconds is sufficient to produce a martensite fraction of 6.9 vol.%. After 1 min, this fraction increased to 24.3%. Then, the austenite growth rate decreases gradually. After 30 min, the equilibrium austenite fraction of 36.6 vol.% at this temperature is almost achieved. The ferrite grain size is again very stable. As in the case of the intercritical annealing temperature, the ferrite grains become more equiaxed when the martensite fraction is increased. The retained austenite fraction is generally very low and does not vary notably with increasing holding time. Again, the highest fraction of HAGBs in ferrite corresponds to the lowest martensite fraction.

In Figs. 5(c) and 5(d), the lower and upper bound experiments are shown. It can be clearly seen that the martensite fraction and the martensite island size increase with increasing holding time. In the sample held for 2 s (Fig. 5(c)), there is some cementite visible that has not yet transformed. In the sample held for 30 min (Fig. 5(d)), the preferred austenite growth direction parallel to the rolling direction becomes visible which results in a higher proportion of interconnected martensite islands.

The effect of isothermal holding time was only studied at a temperature of 730°C, *i.e.*, at a temperature where austenite formation is controlled by carbon diffusion. It was found that phase transformation rate is low in the beginning (2 seconds holding time), experiences a rapid increase up to 300 seconds and then levels off until the maximum holding time of 1 800 seconds, where equilibrium is nearly established, Table 1 and Fig. 4(b). The logarithmic scaling of the time vs. phase fraction function suggests that we observe a sigmoidal curve that is commonly associated with a nucleation and growth process, albeit the number of experimental data is quite limited. The micrograph in Fig. 5(c) reveals that austenite growth is active even during this short intercritical annealing treatment, documenting the dominance of carbon diffusion at this temperature. Nevertheless, austenite growth is restricted at this stage due to the prevailing austenite nucleation.[49] As holding time increases, the phase transformation rate is slower because the preferred cementite nucleation sites are exhausted and austenite growth has to proceed by the slower carbon diffusion through the austenite/ferrite interface.[30] It was found in previous studies that after carbon has reached equilibrium distribution between the phases, further austenite growth requires the partitioning of substitutional elements like Mn and Si.[49] However, previous studies concerning Mn partitioning during intercritical annealing[29,31,49] are based on the assumption of a homogeneous distribution of Mn between ferrite and cementite (or pearlite). Then, Mn partitions from ferrite to austenite during intercritical annealing. Commonly, a Mn-rich rim is observed in the boundary region of the martensite islands.[31] This rim is a result of the low diffusion coefficient of Mn in austenite which is three orders of magnitude lower than in ferrite. Therefore, Mn piles up at the ferrite/austenite interface during partitioning. In the present investigation, the contrary situation is the case. Mn is enriched in cementite before intercritical annealing.[47] It was shown in a previous study[27] that the Mn enrichment is inherited by austenite and is clearly visible inside martensite after quenching. From this observation it is clear, that after equilibrium carbon activity is reached throughout the phases at the given intercritical annealing temperature, Mn has to diffuse from austenite to ferrite to reach the final equilibri-

um. As a consequence of the low diffusion coefficient, this process is not accomplished within the time span investigated. For detailed

It is interesting to note that the equilibrium austenite fraction is only achieved when a sufficient holding time is given. Increasing the holding temperature does not lead to an austenite fraction approximating the equilibrium value. This means that even the fairly high superheating at 750°C and the associated high driving force for phase transformation do not allow an austenite fraction of 30 vol.% to be formed within one minute, whereas a isothermal holding at 730°C for 30 minutes is sufficient to achieve the equilibrium amount of around 37 vol.%. This implies that austenite nucleation and cementite dissolution is proceeding fast at all temperatures, but austenite growth is sluggish and is rather a function of time than of temperature within this intermediate temperature range. There are three reasons for the slow austenite growth. 1) Cementite dissolution proceeds much faster than austenite growth into ferrite[46] due to the slower carbon diffusion through the austenite/ferrite interface. 2) The inherited high Mn content in the premature austenite lowers the carbon activity and therefore, the growth rate. The higher Mn content in austenite was documented in a previous study and clearly demonstrates the difference between a conventional DP steel, in which austenite is hardly enriched in Mn, and our material. 3) In general, a higher superheating promotes nucleation of austenite and hence, faster transformation kinetics. In the present case, however, the high number of potential nucleation sites in the starting material facilitates saturation of the nucleation sites. As a result, a higher superheating does not have the potential of accelerating phase transformation kinetics by a higher number of nucleation sites. Thus, higher annealing temperatures do not change the microstructure evolution significantly when a holding time of 1 min is chosen.

3.3. Effect of Heating Rate

The range of heating rates applied was +0.25 K/s to +100 K/s. The effect on the microstructure evolution is shown in Fig. 4(c). Long reheating times tend to slightly increase the martensite fraction and decrease the ferrite grain size. The ferrite aspect ratio is not influenced by the heating rate (Table 1), as well as the small retained austenite fraction. The fraction of HAGBs in ferrite is nearly constant for low to intermediate heating rate. The sample heated at the fasted rate (+100 K/s), exhibits the lowest fraction of HAGBs of all samples tested. Comparison of Figs. 5(e) and 5(f) reveals that there is no striking difference in the microstructures obtained at the lowest and fastest heating rate applied. However, a closer look reveals that more ferrite grain boundaries are covered by martensite in the sample heated at +100 K/s and that these martensite islands exhibit a rather elongated shape. As will be explained in section 3.6, the preferential growth direction of austenite is along the HAGBs. Due to the shorter holding time above the Ac_1 temperature and the higher degree of superheating, austenite nucleation is promoted rather than austenite growth.[34] Therefore, more HAGBs are covered by austenite and less austenite growth into ferrite takes place. Hence, the fraction of HAGBs in ferrite is reduced, and the ferrite grain size is larger compared to lower heating rates. Although there is no clear tendency of the variation of these parameters with increasing heating rate, it is possible that this trend becomes more obvious at higher heating rates.

The minor influence of the heating rate on the final microstructure is contradictory to the findings by several other authors. For example, Andrade-Carozzo and Jacques[35] found a considerable increase in martensite volume fraction and a decrease in ferrite grain size with increasing heating rate. The authors attribute these microstructural changes to the competitive processes of recrystallization and phase transformation. Slower heating promotes ferrite recrystallization and hence grain growth, whereas fast heating preserves the defect structure of the non-recrystallized ferrite and increases the austenite nucleation rate. However, the authors studied cold-rolled material that has a high driving force for recrystallization. In the material studied here, recrystallization does not occur and ferrite grain growth is suppressed. One could argue that at least the transformation rate should be faster at higher heating rates due to the larger superheating and the facilitation of nucleation, as was reported in Refs..[34,36] However, the authors of these studies investigated ferrite/pearlite starting microstructures, the spacing between pearlite colonies being in the range of several μm. Hence, the number of available nucleation sites is quite limited and consequently, there is a large potential of facilitating nucleation by a large superheating. In contrast, the UFG ferrite/cementite starting microstructure provides a vast amount of potential nucleation sites. Therefore, nucleation site saturation is achieved rapidly during intercritical annealing. Thus, further promotion of austenite nucleation by higher superheating has little effect on the number of austenite grains and thus, on the martensite volume fraction. Given the drastic alterations of the microstructure with the change in heating rate in conventional cold-rolled dual-phase steels, the present starting microstructure seems to be superior in terms of obtaining a fine and uniform distribution of martensite that is nearly invariant to the change in heating rate.

3.4. Effect of Cooling Rate

To test the effect of the cooling rate, samples were heated at an intermediate heating rate of +20 K/s to 730°C, held for 1 min and then cooled at rates between –140 K/s and –20 K/s. During cooling, ferrite grows at the expense of austenite, which is accompanied by an increase in the austenite carbon content. Thus, the higher the cooling rate (*i.e.* the shorter the cooling time between intercritical annealing temperature and room temperature), the higher the martensite fraction and the smaller the ferrite grain size. This tendency is clearly revealed in Fig. 4(d). The micrographs in Figs. 5(g) and 5(h) further show the reduction in martensite fraction when the cooling rate is lowered. Comparing these micrographs, one can see that lowering the cooling rate leads to a finer martensite distribution, *i.e.* the martensite island size is reduced and the percolation of martensite, which occurs occasionally in the rapidly quenched DP steel, is impeded. In the sample cooled at –20 K/s (Fig. 5(h)), some bainitic areas are visible (white arrow), indicating that –20 K/s falls slightly below the critical cooling rate for complete austenite-to-martensite phase transformation. A high martensite fraction again coincides with a more equiaxial

ferrite grain shape, Table 1. The HAGB fraction in ferrite varies between 47% and 57%, but no clear tendency with respect to cooling rate is apparent. As austenite is enriched in carbon during slow cooling, more effective austenite stabilization was anticipated. Indeed, the highest retained austenite fraction (1.7 vol.%) is present in the sample cooled at –20 K/s.

The hardenability of the steel is fairly high: even at a moderate cooling rate of –20 K/s, the main part of the second phase fraction is martensitic. This is surprising not only with respect to the absence of additional alloying elements like Mo or Cr, but also with respect to the small grain size. This issue is addressed in detail in.[27] In general, a coarse grained microstructure exhibits a higher hardenability than a fine grained microstructure.[50] This is because austenite decomposition starts at grain boundaries, and so the higher grain boundary density in ultrafine grains accelerates austenite decomposition. However, it is shown that the enhanced Mn content in cementite is inherited by austenite and increases its hardenability. As a result, the detrimental effect of the high grain boundary density in the ultrafine grained material is balanced by the beneficial effect of a higher Mn content in austenite. Furthermore, the process of carbon enrichment in austenite during slow cooling (due to the growth of ferrite at the expense of austenite) is more effective when the diffusion distances are small, as it is the case in ultrafine grains. Thus, the higher carbon content of the remaining austenite leads to an improved hardenability.

3.5. Grain Size Stability

A comparison between the intercritically annealed steel and the initial UFG ferrite/cementite microstructure (Table 1) reveals that the average ferrite grain size increases from 0.84 μm in the UFG-F/C steel to 1.1–1.4 μm in the UFG DP steels, Table 1. Hence, grain growth during intercritical annealing is largely suppressed in these steels. Several reasons can account for the fairly high grain size stability. 1) The pronounced recovery during large strain warm deformation and warm annealing decreased the dislocation density and therefore, recrystallization and grain growth during intercritical annealing are delayed. 2) The ferrite grain boundaries are effectively pinned by the cementite particles which are located mostly along the grain boundaries. This effect is enhanced by the fairly high Mn content (1.63 wt.%) which was shown to refine the cementite particle size.[47] 3) The growing austenite decelerates the grain boundary migration.[29] 4) The grain boundary mobility is further restricted due to Mn in solid solution which exerts a solute drag effect.[51] 5) Mn contributes to the grain size stability by broadening the ferrite + austenite + cementite three-phase field, in which grain growth is strongly inhibited, and 6) by lowering the Ac_1 temperature, and thereby the grain growth kinetics at the intercritical annealing temperature.

The ferrite grain size varies only slightly in all intercritical annealing setups. There is a tendency of decreasing grain size with increasing intercritical annealing temperature as a result of the higher austenite fraction growing into ferrite. Similarly, decreasing the cooling rate leads to epitaxial growth of ferrite at the expense of austenite and therefore, to a slight increase in grain size with decreasing austenite (martensite) fraction. In contrast, increasing the holding time does not lead to significant changes in ferrite grain size, whereas austenite grows continuously. This indicates that during isothermal holding, ferrite grain growth continues. However, ferrite grain coarsening is balanced by the continuous growth of austenite into the adjacent ferrite. The limited mobility of ferrite grain boundary described above contributes to the stability of the ferrite grain size.

It is interesting to note that the grain size after the shortest investigated intercritical annealing time of 2 seconds increased to 1.17 μm in comparison to 0.84 μm in the initial microstructure. This means that grain growth is relatively fast before the ferrite + cementite $\rightarrow$ austenite transformation occurs. With the onset of austenite formation, ferrite grain growth is slowed down. In contrast to ferrite, the martensite island size increases significantly with increasing holding temperature and holding time, whereas it decreases with decreasing cooling rate.

It must be added that the competing recrystallization process is not regarded in this discussion. It was shown in a previous study,[52] that the recrystallization behavior of this material is quite unlike the one of a conventional cold-rolled dual-phase steel.[53] This is a result of the low dislocation density in the warm deformed ferrite which retards recrystallization. It was concluded from detailed microstructure and texture evaluations that grain growth prevails over recrystallization.

3.6. Microstructure Evolution during Intercritical Annealing

The preferential austenite nucleation sites are the ferrite/cementite interfaces because of the large amounts of carbon being available and because the high interface energy reduces the energy barrier for the formation of an austenite nucleus.[54,55] In the present case, the Mn enrichment in cementite, which takes place during large strain warm deformation,[47] further promotes this nucleation site by lowering the transformation start temperature. The cementite particles located at ferrite grain boundaries are more effective nucleation sites than cementite located inside the ferrite matrix. This is revealed *e.g.* in the micrograph in Fig. 5(f), where some cementite is still present inside the ferrite grains. It is clear that not every cementite particle will form a nucleation site. As described by Hillert *et al.*,[46] austenite first forms a shell around a cementite particle after nucleation owing to the reasons states above. By further carbon diffusion through this shell, the austenite grows. In case of a short distance between cementite particles, diffusion of carbon will additionally take place through ferrite, thereby dissolving the neighboring cementite particles. In this way, rather large austenite grains can grow. This growth process seems to be very effective in the present case, because even after a short intercritical annealing time of 2 seconds, fairly large martensite (formerly austenite) islands are visible, Fig. 5(c). The fact that longer holding times produce a quite homogeneous distribution of austenite (Fig. 5(d)) suggests that nucleation and growth proceed simultaneously throughout the intercritical annealing treatment. Austenite grows both into the ferrite matrix and along the ferrite grain boundaries, the latter being the faster process. For this reason, some of the martensite islands exhibit an elongated shape with the longitudinal axis being commonly aligned with the rolling direc-

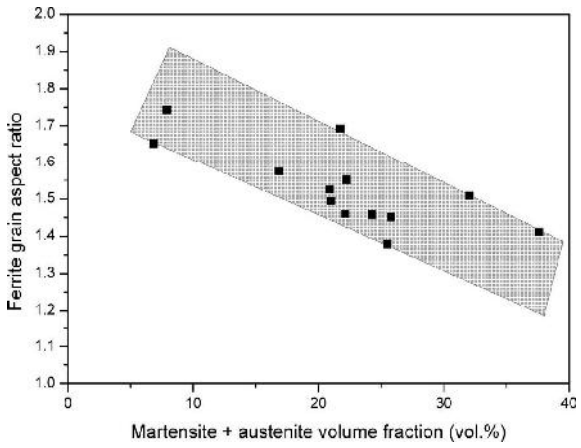

Fig. 6. Ferrite grain aspect ratio as a function of martensite volume fraction. The shaded area highlights the decreasing tendency. Data obtained from samples listed in Table 1.

tion. In this sense, they follow the trace of the cementite particles, which were to some extent aligned in the same direction. The preferential growth along grain boundaries is a consequence of the higher diffusion coefficient that accelerates the growth rate.[29)]

The elongated shape of some martensite islands further leads to the increase in the ferrite grain aspect ratio upon intercritical annealing from around 1.3 to around 1.5. Consistently, there is an overall tendency towards lower ferrite aspect ratios with increasing martensite fraction, *i.e.* with increasing intercritical annealing time and temperature, **Fig. 6**. When grain growth along the rolling direction is saturated, austenite growth continues perpendicular to the rolling direction as holding time is increased. At higher temperatures, grain growth perpendicular to the rolling direction is facilitated due to the higher diffusion coefficients and to the lower carbon content required for austenite formation.

Another important change in microstructural features upon intercritical annealing concerns the fraction of HAGBs in ferrite. The HAGB fraction decreases from around 61% in the initial microstructure to around 49% after intercritical annealing. A possible explanation is that HAGBs are more effective nucleation sites than LAGBs due to their higher energy.[56)] Furthermore, HAGBs constitute easy diffusion paths which are more effective than those in LAGBs.[51)] Therefore, austenite nucleates and grows preferentially along HAGBs, leaving LAGBs more often unaffected. In this way, the fraction of HAGBs in ferrite is reduced.

3.7. Implications for Mechanical Properties

Determining the optimum intercritical annealing parameters means deciding which microstructure is most promising for commercial applications in terms of strength, ductility and formability. In principal, the martensite volume fraction should be kept below 30 vol.% in order to maintain an appropriate ductility. Moreover, martensite percolation should be avoided as martensite bands lead to high local stress accumulations and early failure of martensite islands which results in a reduced tensile ductility.[8)] However, a sufficiently high martensite fraction is essential for obtaining high strength levels. Strengthening coefficients of 8.5–13 MPa/(vol.% martensite) have been reported.[57)] Furthermore, the strain hardening rate was shown to increase with increasing martensite volume fraction.[58)] On the other hand, total elongation is reduced when the martensite volume fraction is increased.[59)] The intercritical annealing parameter that has the largest effect on martensite volume fraction is the holding time. It was found that a holding time of 1 min was sufficient for dissolving all cementite particles and to achieve a martensite fraction in the desired range. As an optimum intercritical annealing temperature, the minimum temperature that produces a cementite-free microstructure was chosen. Under the present conditions, this requirement is fulfilled at 730°C. The heating rate does not have a crucial influence on the microstructure evolution within the investigated range (+0.25 to +100 K/s). Concerning the cooling rate, it was often shown that intermediate cooling yield better combination of strength and ductility compared to rapidly quenched counterparts (*e.g.*[28,57,60)]). In general, uniform and total elongation are both increased whereas the ultimate tensile strength is decreased when the cooling rate is lowered. The increase in ductility is attributed to the more ductile ferrite, which is depleted from supersaturated interstitial carbon upon slow cooling, thus becoming softer.[60)] Additionally, the increasing fraction of retained austenite stemming from the higher carbon content in austenite was shown to be important for the improved ductility.[61)] In the present case, slower cooling leads to the break-up of large martensite islands and martensite bands, hence, yielding a fine martensite distribution that cannot be achieved by lowering the intercritical annealing temperature or holding time. Generally, a fine martensite dispersion is desirable for good formability properties.

4. Conclusions

A plain C–Mn steel with an ultrafine grained ferrite/cementite microstructure was subjected to intercritical annealing to obtain an ultrafine grained ferrite/martensite microstructure. The intercritical annealing conditions were varied in order to study the mechanisms that control microstructure evolution. The main conclusions are:

- During intercritical annealing, the ferrite grain size is slightly increased from ~0.8 μm to ~1.2 μm. The high grain size stability is explained by the absence of recrystallization, the effective pinning by grain boundary cementite particles, the broadening of the ferrite + austenite + cementite three-phase field by Mn and the restricted grain boundary mobility due to Mn in solid solution.
- Austenite nucleation and growth occur concurrently throughout the intercritical annealing treatment. Preferred austenite growth along grain boundaries aligned with the rolling direction leads to an increase in ferrite aspect ratio from ~1.3 to ~1.5 after intercritical annealing.
- The HAGB fraction is reduced upon intercritical annealing from ~60% to ~50%. This is possibly due to the preferential austenite nucleation at HAGBs as a result of their higher energy.
- Increasing the isothermal holding time exerts a stronger effect on austenite growth than increasing the intercritical annealing temperature. This is explained by the

slow Mn diffusion controlled phase transformation at low temperatures and by the high Mn content in austenite that lowers carbon activity and thus austenite growth rate. Hence, to achieve the equilibrium austenite fraction, a fairly long intercritical annealing treatment (30 minutes) at a temperature where phase transformation is controlled by carbon diffusion (> 710°C) is required.

- The microstructure is nearly indifferent to changes in heating rate. The larger superheating at high heating rates does not influence the phase transformation kinetics significantly as a result of fast nucleation site saturation.
- Lowering the cooling rate leads to epitaxial growth of ferrite at the expense of austenite and thus to a finer martensite distribution that is accompanied by a slight increase of the ferrite grain size.
- The ferrite grain size is largely insensitive to changes in heating rate, holding time and temperature. This is basically explained by the simultaneous growth of ferrite and austenite.
- A holding temperature of 730°C and a holding time of 1 minute are most suitable to obtain a cementite-free ferrite/martensite microstructure. At the fastest quench rate (–140 K/s) and an intermediate heating rate (–20 K/s), this microstructure contains 24.3 vol.% martensite, the ferrite grain size being 1.2 μm. A small fraction of retained austenite (1.2 vol.%) occurs mainly as interlath austenite inside the martensite islands and to a less extent as isolated grains. Martensite islands are mainly isolated and have approximately the same size as ferrite.

REFERENCES

1) R. Song, D. Ponge, D. Raabe, J. G. Speer and D. K. Matlock: *Mater. Sci. Eng. A*, **441** (2006), 1.
2) K. T. Park, Y. S. Kim, J. G. Lee and D. H. Shin: *Mater. Sci. Eng. A*, **293** (2000), 165.
3) N. Tsuji, N. Kamikawa, R. Ueji, N. Takata, H. Koyama and D. Terada: *ISIJ Int.*, **48** (2008), 1114.
4) H. Azizi-Alizamini, M. Militzer and W. J. Poole: *Scr. Mater.*, **57** (2007), 1065.
5) Z. L. Zhang, Y. N. Liu, J. W. Zhu and Y. U. Guang: *Mater. Sci. Forum*, **551–552** (2007), 199.
6) S. Murty and S. Torizuka: *ISIJ Int.*, **48** (2008), 1088.
7) Y. I. Son, Y. K. Lee, K. T. Park, C. S. Lee and D. H. Shin: *Acta Mater.*, **53** (2005), 3125.
8) M. Calcagnotto, D. Ponge and D. Raabe: *Mater. Sci. Eng. A*, **527** (2010), 7832.
9) R. G. Davies: *Metall. Trans. A*, **9** (1978), 41.
10) J. M. Rigsbee and P. J. Vander Arend: Formable HSLA and Dual-phase Steels, ed. by A. D. Davenport, The Metallurgical Society of AIME, New York, USA, (1979), 58.
11) G. R. Speich: Fundamentals of Dual-phase Steels, ed. by R. A. Kot and B. L. Bramfitt, The Metallurgical Society of AIME, New York, USA, (1981), 3.
12) N. K. Balliger and T. Gladman: *Met. Sci.*, **15** (1981), 95.
13) D. L. Bourell and A. Rizk: *Acta Metall.*, **31** (1983), 609.
14) A. M. Sarosiek and W. S. Owen: *Mater. Sci. Eng.*, **66** (1984), 13.
15) Y. L. Su and J. Gurland: *Mater. Sci. Eng.*, **95** (1987), 151.
16) P. H. Chang and A. G. Preban: *Acta Metall.*, **33** (1985), 897.
17) Z. H. Jiang, Z. Z. Guan and J. S. Lian: *Mater. Sci. Eng. A*, **190** (1995), 55.
18) M. Sarwar and R. Priestner: *J. Mater. Sci.*, **31** (1996), 2091.
19) O. Bouaziz, T. Iung, M. Kandel and C. Lecomte: *J. Phys. IV*, **11** (2001), 223.
20) K. P. Imlau and T. Heller: *Steel Res. Int.*, **78** (2007), 180.
21) M. Calcagnotto, Y. Adachi, D. Ponge and D. Raabe: *Acta Mater.*, **59** (2010), 658.
22) M. Calcagnotto, D. Ponge, E. Demir and D. Raabe: *Mater. Sci. Eng. A*, **527** (2010), 2738.
23) M. Delincé, P. J. Jacques and T. Pardoen: *Acta Mater.*, **54** (2006), 3395.
24) M. Delincé, Y. Brechet, J. D. Embury, M. G. D. Geers, P. J. Jacques and T. Pardoen: *Acta Mater.*, **55** (2007), 2337.
25) K. Mukherjee, S. S. Hazra and M. Militzer: *Metall. Mater. Trans. A*, **40** (2009), 2145.
26) M. Calcagnotto, D. Ponge and D. Raabe: *ISIJ Int.*, **48** (2008), 1096.
27) M. Calcagnotto, D. Ponge and D. Raabe: *Metall. Mater. Trans. A*, **43** (2011), 37.
28) D. K. Matlock, G. Krauss, L. F. Ramos and G. S. Huppi: Structure and Properties of Dual-phase Steels, ed. by R. A. Kot and J. W. Morris, The Metallurgical Society of AIME, New York, USA, (1979), 62.
29) C. I. Garcia and A. J. DeArdo: *Metall. Trans. A*, **12** (1981), 521.
30) P. Messien, J. C. Herman and T. Gréday: Fundamentals of Dual-phase Steels, ed. by R. A. Kot and B. L. Bramfitt, The Metallurgical Society of AIME, New York, USA, (1981), 161.
31) G. R. Speich, V. A. Demarest and R. L. Miller: *Metall. Trans. A*, **12** (1981), 1419.
32) C. Atkinson, T. Akbay and R. C. Reed: *Acta Metall. Mater.*, **43** (1995), 2013.
33) M. H. Saleh and R. Priestner: *J. Mater. Process. Technol.*, **113** (2001), 587.
34) J. Huang, W. J. Poole and M. Militzer: *Metall. Mater. Trans. A*, **35** (2004), 3363.
35) V. Andrade-Carozzo and P. J. Jacques: *Mater. Sci. Forum*, **539–543** (2007), 4649.
36) F. L. G. Oliveira, M. S. Andrade and A. B. Cota: *Mater. Charact.*, **58** (2007), 256.
37) R. Kaspar and O. Pawelski: *Materialprüfung*, **31** (1989), 14.
38) O. Pawelski and R. Kaspar: *Materialprüfung*, **30** (1988), 357.
39) R. Song, D. Ponge, D. Raabe and R. Kaspar: *Acta Mater.*, **53** (2005), 845.
40) J. S. Distl, A. Streißelberger, R. Kaspar and U. Zeislmair: *Materialprüfung*, **27** (1985), 131.
41) A. W. Wilson, J. D. Madison and G. Spanos: *Scr. Mater.*, **45** (2001), 1335.
42) T. Waterschoot, L. Kestens and B. C. De Cooman: *Metall. Mater. Trans. A*, **33** (2002), 1091.
43) J. H. Wu, P. J. Wray, C. I. Garcia, M. J. Hua and A.J. DeArdo: *ISIJ Int.*, **45** (2005), 254.
44) Y. Qiao: *Mater. Sci. Eng. A*, **361** (2003), 350.
45) B. Jansson, M. Schalin, M. Selleby and B. Sundman: Computer Software in Chemical and Extractive Metallurgy, ed. by C. W. Bale and G. A. Irons, The Metallurgical Society of CIM, Quebec, Canada, (1993), 57.
46) M. Hillert, K. Nilsson and L. E. Torndahl: *J. Iron Steel Inst.*, **209** (1971), 49.
47) R. Song, D. Ponge and D. Raabe: *ISIJ Int.*, **45** (2005), 1721.
48) G. R. Purdy, D. H. Weichert and J. S. Kirkaldy: *Trans. TMS-AIME*, **230** (1964), 1025.
49) P. Wycliffe, G. R. Purdy and J. D. Embury: Fundamentals of Dual-phase Steels, ed. by R. A. Kot and B. L. Bramfitt, The Metallurgical Society of AIME, New York, USA, (1981), 59.
50) Werkstoffkunde, ed. by H. J. Bargel and G. Schulze, Springer, Berlin, Germany, (1999).
51) D. A. Porter, K. E. Easterling and M. Y. Sherif: Phase transformations in metals and alloys, CRC Press, Taylor & Francis Group, Boca Raton, USA, (2009).
52) M. Calcagnotto: Ultrafine grained dual-phase steels, Shaker, Aachen, Germany, (2011).
53) T. Ogawa, N. Maruyama, N. Sugiura and N. Yoshinaga: *ISIJ Int.*, **50** (2010), 469.
54) J. W. Cahn: *Acta Metall.*, **7** (1959), 18.
55) K. C. Russell and H. I. Aaronson: *J. Mater. Sci.*, **10** (1975), 1991.
56) J. Becker and E. Hornbogen: Structure and properties of Dual-phase Steels, ed. by R. A. Kot and J. W. Morris, The Metallurgical Society of AIME, New York, USA, (1979), 20.
57) S. S. Hansen and R. R. Pradhan: Fundamentals of Dual-phase Steels, ed. by R. A. Kot and B. L. Bramfitt, The Metallurgical Society of AIME, New York, USA, (1981), 113.
58) B. Karlsson and B. O. Sundström: *Mater. Sci. Eng.*, **16** (1974), 161.
59) G. R. Speich and R. L. Miller: Structure and Properties of Dual-phase Steels, ed. by R. A. Kot and J. W. Morris, The Metallurgical Society of AIME, New York, USA, (1979), 145.
60) S. Hayami, T. Furukawa, H. Gondoh and H. Takechi: Formable HSLA and Dual-phase Steels, ed. by A. D. Davenport, The Metallurgical Society of AIME, New York, USA, (1979), 167.
61) T. Furukawa, H. Morikawa, H. Takechi and H. Koyama: Structure and Properties of Dual-phase Steels, ed. by R. A. Kot and J. W. Morris, The Metallurgical Society of AIME, New York, USA, (1979), 281.